Int. J. Electrochem. Sci., 14 **(2019)** 2645 – 2654, doi: 10.20964/2019.03.10

International Journal of
ELECTROCHEMICAL
SCIENCE
www.electrochemsci.org

Improved Oxidative Cleavage of Lignin Model Compound by ORR in Protic Ionic Liquid

Haomin Jiang, Lei Wang, Lingling Qiao, Aiguo Xue, Yujuan Cheng, Yueying Chen, Yuan Ren, Yongmei Chen, and Pingyu Wan**

Institute of Applied Electrochemistry, Faculty of Science, Beijing University of Chemical Technology, 100029 Beijing, P. R. China
*E-mail: chenym@mail.buct.edu.cn, pywan@mail.buct.edu.cn

Received: 5 November 2018 / *Accepted:* 22 December 2018 / *Published:* 7 February 2019

The electrochemical degradation of *p*-benzyloxyl phenol (PBP) in $[HNEt_3][HSO_4]$ is investigated using an oxygen reductive reaction (ORR) cathode in a non-membrane cell. It is disclosed that the two-electron reductive products of O_2 (that is H_2O_2) is the main reactive oxygen species (ROS) in $[HNEt_3][HSO_4]$, a protic ionic liquid (PIL). The degradation of PBP in PIL with the degradation rate of 48.2% and the current efficiency of 29.5% are obtained, which is higher than that in $[BMIM][BF_4]$, an aprotic ionic liquid (AIL). Based on the products identified by GC-MS, the effect of electro-generated H_2O_2 on the cleavage of ether bond in PBP is proposed. The result confirms that the appropriate number of protons in supporting electrolyte plays an important role in electrochemical degradation of lignin model compounds.

Keywords: *p*-benzyloxyl phenol (PBP), oxygen reduction reaction (ORR), protic ionic liquid (PIL), lignin depolymerization, reactive oxygen species (ROS)

1. INTRODUCTION

Lignin accounts for about 15%-30% of lignocellulose biomass, and it is the unique natural products with aromatic structure. Lignin possesses huge molecular weight with structural units of syringyl, guaiacyl and p-hydroxyphenyl [1]. The degradation of lignin into mono-benzene compounds, such as vanillin and syringaldehyde, is thought to be feasible utilization of lignin [2-5]. Many methods have been reported to degrade lignin, such as hydrogenlysis[6-8], pyrolysis [9-12] and oxidation methods [13-15]. However, the reactions need harsh conditions or expensive catalysts and amounts of regents. Electrochemical method [16-18] is thought to be an attractive path because it does not need extra regents and the degradation rate could be controlled by carefully controlling the electrolysis conditions [19-21].

In the reported studies on lignin degradation by electrochemical method, most researchers focused on oxidative degradation of lignin or lignin model compounds by DSA anode, such as IrO_2, PbO_2[22-27]. However, the degradation rate is limited due to the low diffusion rate of lignin molecules to the anode surface, and the depolymerized products might be over-oxidized to aromatic acids due to the high potential on anode.

We first proposed that electrochemical degradation of lignin by an oxygen reductive reaction (ORR) cathode, on which the reactive oxygen species (ROS, such as H_2O_2, ·OH, $\cdot O_2^-$, $HO_2\cdot$) are generated in situ take parts in the cleavage of alkyl-O-aryl bonds in lignin [28-30]. It is believed that the number and lifetime of ROS is the key factor for improving the degradation rate and current efficiency. Many studies disclosed that the lifetime of ROS generated by ORR cathode was prolonged in ILs [31-35]. Our previous study confirmed that the degradation rate and the current efficiency greatly increased in $[BMIM][BF_4]$ (an aprotic ionic liquid, AIL) comparing with that in aqueous system [36]. It was also found that the degradation rate could further increase if trace amount of water was added into AIL. Other studies have confirmed that the reduction of O_2 on cathode undergoes two-electron-reduction to form H_2O_2 upon the addition of H_2O into AILs, and the presence of H^+ transport reactions was confirmed to be beneficial to the H_2O_2 reaction pathway [37-40]. We proposed that the higher degradation rate was attributed to the better oxidation capability of H_2O_2 than $\cdot O_2^-$, which inspires us to make sure the effect of protons on the direct formation of H_2O_2 in protic ionic liquid.

Here we report the study of electrochemical behaviors of ORR in a protic IL, $[HNEt_3][HSO_4]$, and the effect on the electrochemical degradation of PBP is also tested.

2. EXPERIMENTAL

2.1. Chemicals and reagents

PBP (≥ 99%) was purchased from J&K Scientific (Beijing, China) and $[HNEt_3][HSO_4]$ was synthesized following the published method [41]. The molecular structures of PBP and the IL are given in Scheme 1. Prior to the electrochemical experiment, the prepared ILs was dried at 80°C under vacuum conditions for 48h. Silver nitrate for the fabrication of a reference electrode was obtained from Alfa Aesar (Shanghai, China), and other chemicals such as diethyl ether and acetonitrile were obtained from Beijing Chemical Reagents Company (Beijing, China).

2.2. Electrochemical study

The cyclic voltammetry (CV) curves were recorded on an electrochemical workstation (CHI660E, CH Instruments Ins. USA) by using a three-electrode-system in an undivided electrolytic cell: a glassy carbon electrode (GCE, 3 mm in diameter) as the working electrode, a platinum sheet (10 mm × 10 mm) as the counter electrode, and an IL-based Ag/Ag^+ quasi-reference electrode (Ag/10 mM $AgNO_3$ in acetonitrile) [42] as the reference electrode. The mixture of $[HNEt_3][HSO_4]$ and acetonitrile (1:6 in mass) with or without 10 mM PBP was used as the supporting electrolyte. Prior to CV measurement, the electrolyte was bubbled with N_2 or O_2 for 30 min and kept bubbling during the test.

The number of transferring electrons (*n*) was determined by the rotating ring-disk electrode (RRDE) technique. It was carried out on an electrochemical equipment (Pine Instrument Company, USA) in standard three-electrode system. A rotating ring-disk electrode (GC disk with Pt ring, 5.61 mm in diameter for the disk) was used as the working electrode. A platinum wire and the as-prepared Ag/Ag^+ quasi-reference electrode was served as the counter electrode and the reference electrode, respectively. The disk potential was scanned from 0 V to -1.5 V with a scanning rate of 5 mV s^{-1} in O_2-saturated electrolyte, and the ring potential was controlled at 0.2 V (vs. Ag/Ag^+, the same hereafter), and the rotating speed of disk and ring were kept at 1600 rpm. Then the number of transferring electrons of ORR is calculated by eq (1):

$$n = \frac{4I_\mathrm{d}}{(I_\mathrm{r}/N)+I_\mathrm{d}} \quad (1)$$

where I_d and I_r are the current intensity of disk and ring, respectively, and *N* is the collection efficiency, which is evaluated as 0.37 ± 0.01 in this case.

2.3. Electrolysis of PBP

The procedure of continuous electrolysis of PBP followed the procedure that has been described in our previous study [36]. The distance between the graphite felt cathode and RuO_2 -IrO_2/ Ti anode was 40 mm. 5 mmol L^{-1} PBP in the $[HNEt_3][HSO_4]$-acetonitrile m ixed solution (1: 6 in mass) was served as the supporting electrolyte. Electrolysis was carried out under O_2 atmosphere (or N_2 atmosphere as comparison) at 20 - 80°C under current density of 0.4 - 1.3 mA cm^{-2} for 1 - 4 hrs.

2.4. Calculation of current efficiency

The current efficiency (η) for the degradation of PBP is defined as the ratio of the amount of degraded PBP (in mole) to the actual consumed number of electrons (in mole), as expressed by Eq 2:

$$\eta = n_D/n_e = \frac{c_0 \times V \times D \times F}{1000 \times Q} \quad (2)$$

where n_D (mol) and n_e (mol) represent for the degraded PBP and the consumed electrons after electrolysis. c_0 (mmol L^{-1}) is the initial concentration of PBP, *V* (L) is the volume of the electrolyte, *D* (%) is the degradation rate of PBP which is calculated based on the HPLC data, *F* (C mol^{-1}) is Faraday constant, and *Q* (C) is the applied electric quantity, which is calculated as the product of current density (*I*) and electrolytic time (*t*).

2.5. Products analysis by GC-MS and HPLC measurements

The extractive of degradation products by ethyl ether were analyzed by a Shimadzu QP 2010 Plus gas chromatography-mass spectrometer (GC-MS) equipped with a DB-5 MS capillary column (30 m × 0.25 mm × 0.25 μm). 1 μL of sample was injected into the splitless injector at 280°C. Helium gas was used as the carrier gas at a column flow rate of 1.74 mL min^{-1}. The following temperature programming was used: initial column temperature of 45 °C was kept for 5 min and then rise to 110 °C

at 12 °C min^{-1}, after staying at 110 °C for 1 min, the temperature was increased to 280 °C at a rate of 8 °C min^{-1} and then kept for 1 min.

The reaction liquid after electrolysis was directly analyzed by high performance liquid chromatography (HPLC, Dionex Ultimate 3000) equipped with a phenyl column (Waters Xbridge, 5 μm, 4.6 mm × 250 mm). The mobile phase was the mixture of methanol and water (80 : 20 in volume) with flow rate of 0.5 mL min^{-1}.

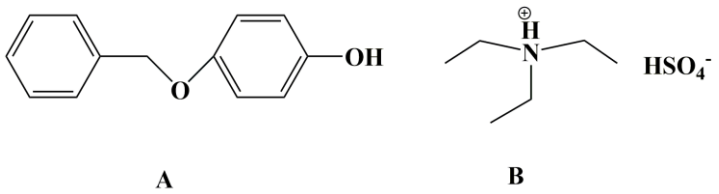

Scheme 1. Molecular structures of (A)PBP ; and (B) $[HNEt_3][HSO_4]$

3. RESULTS AND DISCUSSION

3.1. Electrochemical behaviors of ORR in $[HNEt_3][HSO_4]$ with or without PBP

The CV curves of GCE in supporting electrolyte without PBP under N_2 or O_2 atmosphere (black and red dotted line in Fig. 1A) indicate that the electrochemical reduction of O_2 occurs at potential near -1.28V (marked as peak **2c**). As known from the CV curve in presence of PBP under N_2 atmosphere (black solid line in Fig. 1A), the appearance of anodic peak around 0.51V (peak **1a**) and the cathodic peak at -0.45V (peak **1c**) is confirmed to be related to the electrode reactions of PBP itself.

To further identify the origin of peak **1a** and **1c**, CV curves of GCE in electrolyte with PBP under N_2 atmosphere were performed by negatively scanning started from the open circuit potential. There is no any peak appears in potential range from -0.065 V to -1.50V (red line in Fig. 1B). But an anodic peak at 0.51 V appears in the following positive-going scan (blue line in Fig. 1B), which could attribute to the oxidative reaction of PBP on the anode. Then a cathodic peak at -0.45 V (peak **1c**) is observed in the following negative-going scan (green line in Fig. 1B), which should be assigned to the reductive reaction of the oxidation products of PBP since it only appeared after the occurrence of peak **1a**.

Specifically, totally one anodic peak and two cathodic peaks are observed in CV curve in the presence of PBP under O_2 atmosphere (red solid line in Fig. 1A). The potentials of these peaks did not change, but the intensity of the peak **1c** increased and the peak **2c** decreased. This phenomenon implies that part of PBP in electrolyte was reduced by the ROS generated from ORR.

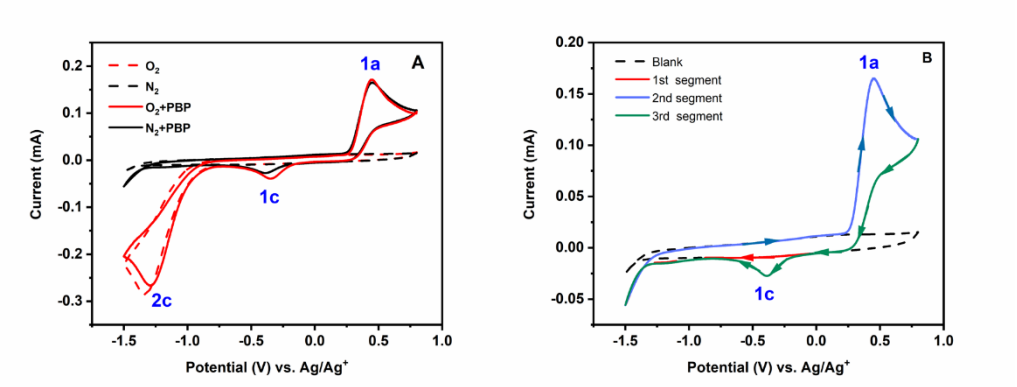

Figure 1. (A) CV curves of GCE in $[HNEt_3][HSO_4]$ without PBP under N_2 atmosphere (black dotted), without PBP under O_2 atmosphere (red dotted), with PBP under N_2 atmosphere (black solid), with PBP under O_2 atmosphere (red solid), scanning rate: 50 mV s^{-1} ; (B) CV curves of GCE in $[HNEt_3][HSO_4]$ with PBP under N_2 atmosphere, negatively scanning started from the open circuit potential of -0.065V to -1.5V (red line), then positive-going to 0.80V(blue line) and finally negative-going to -1.5V (green line), scanning rate: 50 mV s^{-1}

The CV curves of GCE in electrolyte in presence of PBP under O_2 atmosphere with different scanning rates are shown in Fig. 2A. Linear fit of the peak current (I_p) to the sweep rate (v) or the square root of sweep rate ($v^{1/2}$) was performed for each peak. Comparing with the results shown in Fig. 2B and Fig. 2C, it is demonstrated that better linear relationship lies in I_p -$v^{1/2}$ for these three peaks, which indicates that all these electrode reaction processes are diffusion-controlled process. That is to say, the rate of ORR process (peak **2c**) is controlled by the diffusion of the dissolved oxygen molecules to the surface of the working electrode, and the rate of oxidation of PBP (peak **1a**) and the reductive of the oxidation product (peak **1c**) is dependent on the diffusion of the reactants to the surface of the electrode.

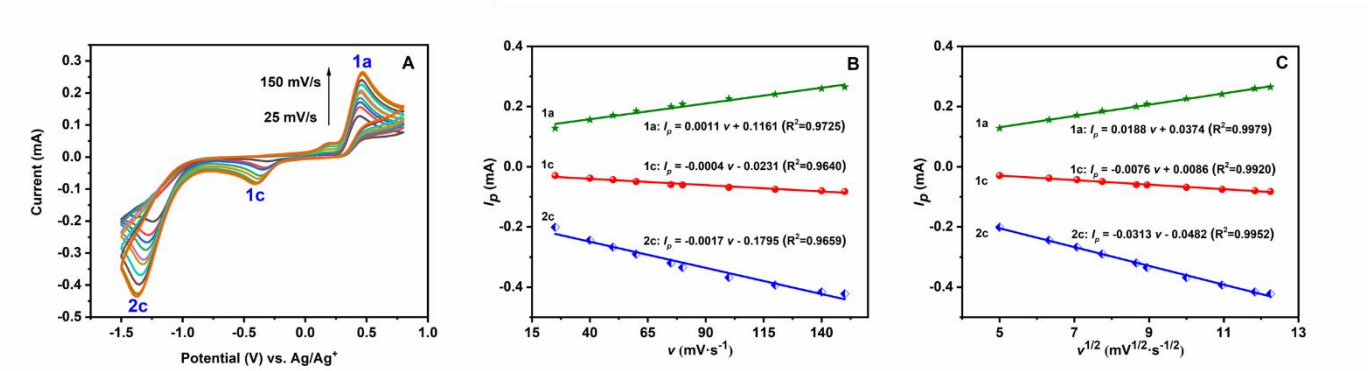

Figure 2. (A) CV curves of GCE in electrolyte with PBP under O_2 atmosphere with scanning rate of 25, 40, 50, 60, 75, 80, 100, 120, 140, 150 mV s^{-1}, respectively; (B) the linear relationship of I_p vs v and (C) the linear relationship of I_p vs $v^{1/2}$ for peak 1a, 1c and 2c, respectively

The rotating ring-disk electrode (RRDE) technique was adopted to investigate the number of transferring electrons during ORR in $[HNEt_3][HSO_4]$. As shown in Fig. 3A, it is demonstrated that there is no significant change in the intensity of disk current and ring current in presence of PBP or not.

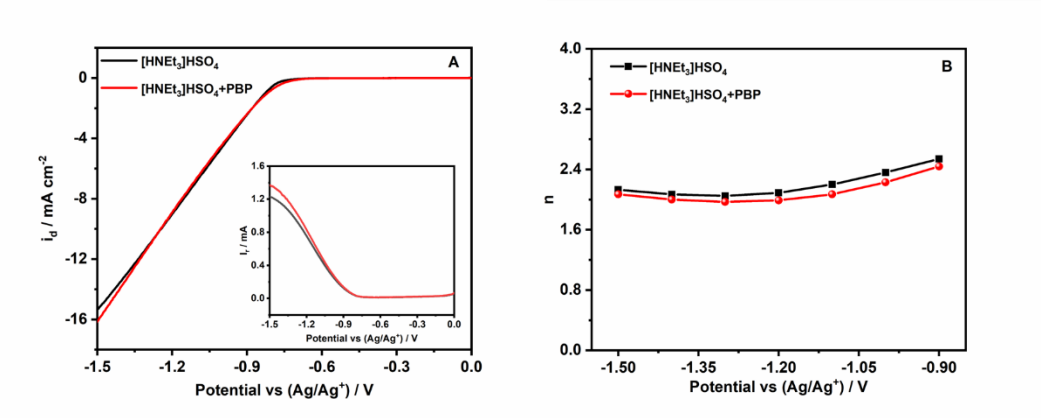

Figure 3. (A) The *I-V* curves of RRDE in $[HNEt_3][HSO_4]$ with or without PBP with rotation speed of 1600 rpm, the inset is the corresponding ring current recorded at potential of 0.2V. (B) The calculated transferring electron numbers for ORR based on RRDE curves

As shown in Fig. 3B, the calculated transferring electron numbers for ORR in $[HNEt_3][HSO_4]$ is around 2.0-2.3, no matter PBP is present or not. It is suggested that ORR follows the electrochemical-chemical-electrochemical-chemical (ECEC) mechanism [43], as described in following Eq 3-6:

$$O_2 + e \leftrightarrow \cdot O_2^- \quad (3)$$

$$\cdot O_2^- + H^+ \leftrightarrow \cdot HO_2 \quad (4)$$

$$\cdot HO_2 + e \leftrightarrow HO_2^- \quad (5)$$

$$HO_2^- + H^+ \leftrightarrow H_2O_2 \quad (6)$$

3.2. The degradation products of PBP

The degradation products of PBP after it was electrolyzed under O_2 atmosphere were analyzed by GC-MS, and benzyl alcohol, benzaldehyde and benzoquinone have been identified (as shown in Fig.4).

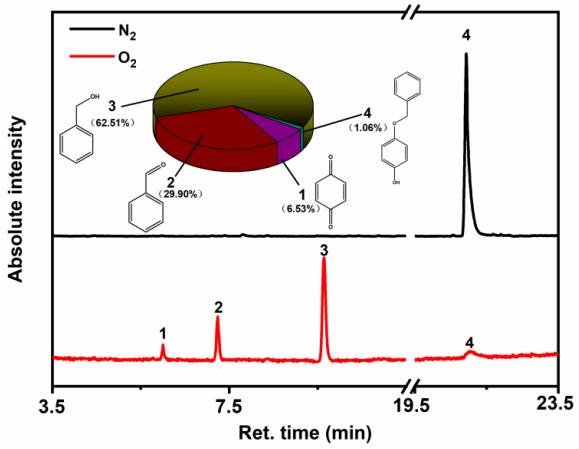

Figure 4. Gas chromatograms of the ether extractive of the reaction liquid after PBP electrochemically degradation on O_2 or N_2 atmosphere

Based on the above discussions, the mechanism of electrochemical degradation of PBP in PIL can be inferred as follows (sketched in Scheme 2): firstly, PBP molecules in PIL dissociate and release one proton per molecule to form phenolate ions (PBP^-), and the latter diffuse to the electrode and donate one electron per molecule at about 0.51V (peak **1a**) forming phenoxy radicals (PBP·) or the corresponding quinone resonance structure. The small parts of PBP· radicals recover to PBP^- during the subsequent reverse scan (peak **1c)**, while the other PBP· radicals homogeneously react with the ROS (mainly H_2O_2) generated by ORR process (see Scheme 2), leading to the formation of benzyl alcohol and benzoquinone. Some benzaldehyde is produced due to further oxidation of benzyl alcohol by ROS.

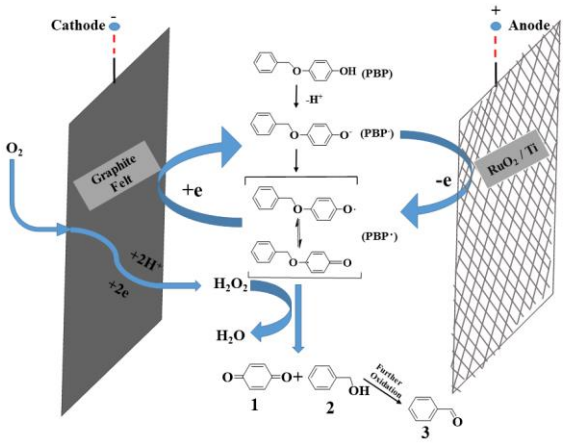

Scheme 2. Scheme of the cleavage of ether-bond in PBP by ORR in PIL.

3.3. The continuous electrolysis of PBP in [HNEt$_3$][HSO$_4$]

The degradation rate and the current efficiency of electrolyzing PBP in [$HNEt_3$][HSO_4] under different operation conditions are shown in Fig. 5.

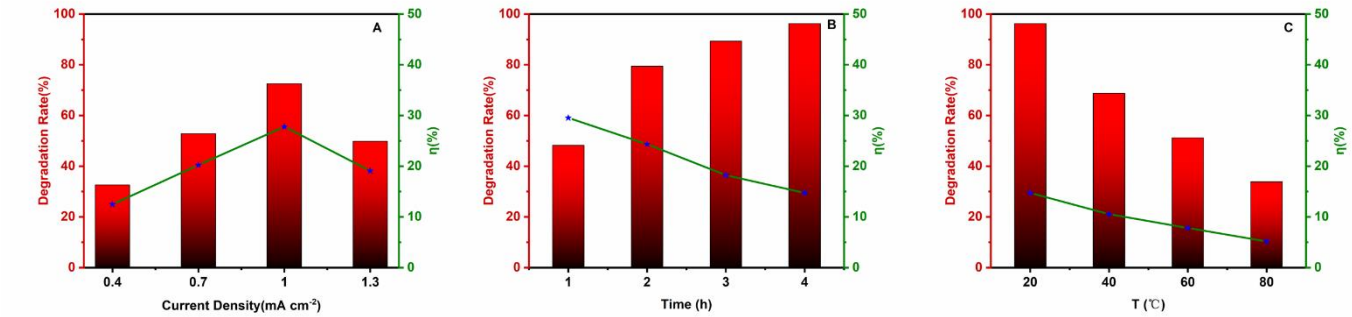

Figure 5. The degradation rate and the current efficiency of electrolyzing PBP in [$HNEt_3$][HSO_4], (A) under different current density but applying the same electric quantity at 20°C; (B) for 1-4 hrs under 1 mA cm^{-2} at 20°C; (C) at different temperature under 1 mA cm^{-2} for 4 hrs.

The effect of current density under the condition of the same applied electric quantity (50.4 C) is shown in Fig. 5A, the highest degradation rate and current efficiency is obtained under the current

density of 1.0 mA cm^{-2}. It was found that the cathodic potentials were -0.54 V, -0.97 V, -1.25 V and -1.62 V when the electrolysis was performed under current densities of 0.4, 0.7, 1.0 and 1.3 mA cm^{-2}, respectively. Since the most feasible potential for ORR in $[HNEt_3][HSO_4]$ is around -1.28 V, it could be explained that the current efficiency increases because of more ROS is produced under the current density of 1.0 mA cm^{-2}.

As shown in Fig. 5B, 48.2% of PBP has been degraded in 1 h with the current efficiency of 29.5%. As the electrolysis time prolonged to 4 hrs, the degradation rate up to 96.2% but the current efficiency decreases to 14.7%. The decrease in current efficiency may be because that the amount PBP in the electrolyte is less and less, and most of the generated ROS is self-consumed.

It is discovered that the degradation rate and the current efficiency decreases as the temperature increases from 20°C to 80°C (as shown in Fig.5C). This may be the result that the lifetime of ROS are shortened as the temperature rises, which has been confirmed in Wu's study [44].

The contrast test of the electrochemical degradation of PBP in an aprotic IL ($[BMIM][BF_4]$) under the same amount of applied electric quantity (that is 50.4C) were performed. It was found that only 23.7% of PBP was degraded with the current efficiency of 7.3%. The reason is assigned to the proper number of protons present in the electrolyte which promotes the formation of H_2O_2 as the main ROS in the system. The generated H_2O_2 possesses appropriate oxidation capacity which attacks the ether bond of PBP in homogeneous phase, resulting in the improvement of the degradation rate and current efficiency.

The comparison of this work with the recently reported studies on electrochemical degradation of lignin or lignin model compounds is listed in Tab 1. It is found that the electrolysis by direct anodic oxidation needed longer time and higher voltage, while most of the current efficiency of these studies were not mentioned (No. 1-5 in Tab 1). By introducing ORR into the electrolysis system, the cell voltage decreases to below 2.0V in alkali aqueous (No. 6 and No.9 in Tab 1), and the current efficiency further increases to about 7% using ILs as supporting electrolyte. The current efficiency is up to 29.5% in this work because H_2O_2 becomes the main ROS of ORR process in PIL, and H_2O_2 is the more effective reagent for cleavage of ether bonds in lignin.

Table 1. The comparison of the reported electrochemical degradation of lignin or lignin model compounds in references.

No	Substrate	Cathode	Anode	Electrolyte	Conditions	DR* (%)	CE** (%)	Ref
1	Lignin	Pt wire coil	Ti/RuO_2-IrO_2	0.5 M NaOH	500 mA/cm^2, 1 h	-	-	22
2		Pt wire coil	$Ti/TiO_2NT/PbO_2$	0.5 M NaOH	100 mA/cm^2, 8 h	64.6	-	23
3		Graphite	$Ti/Sb\text{-}SnO_2$	0.5 M Na_2SO_4	13 mA/cm^2, 3 h	16.5	-	24
4		Graphite	Ti/PbO_2	0.5 M Na_2SO_4	13 mA/cm^2, 3 h	25.6	-	24
5		Pt wire mesh	$Ru_{0.25}V_{0.05}Ti_{0.7}O_x$	PIL	1.5 V, 8 h	6.0	-	25
6		Graphite Felt	RuO_2 –IrO_2/ Ti	1 M NaOH	8 mA/cm^2, 1 h	59.2	-	30
7		Vitreous Carbon	Vitreous Carbon	PIL-H_2O_2	2.5 V, 24 h	51.0	-	40
8		Vitreous Carbon	Vitreous Carbon	AIL-H_2O	2.5 V, 24 h	19.0	-	40
9	Lignin model compounds	C-PTFE gas diffusion electrode	RuO_2 –IrO_2/ Ti	1 M NaOH	4 mA/cm^2, 1 h	40.5	5.4	28
10		C-PTFE gas diffusion electrode	RuO_2 –IrO_2/ Ti	AIL	0.4 mA/cm^2, 1 h	23.7	7.3	36
11		Graphite Felt	RuO_2 –IrO_2/ Ti	PIL	1.0 mA/cm^2, 1 h	48.2	29.5	This work

* Degradation Rate; ** Current Efficiency

4. CONCLUSIONS

The degradation of PBP is studied in $[HNEt_3][HSO_4]$ using an ORR cathode in a non-membraned cell. It is found that 48.2% of PBP can be degraded under current density of 1 mA cm^{-2} for 1 h at 20°C, and the current efficiency is calculated as 29.5%. The electrochemical behaviors of ORR in $[HNEt_3][HSO_4]$ indicate that H_2O_2 is the main generated ROS by ORR in this kind of PIL. The better electrochemically degradation of PBP in PIL than that in AIL is contributed to the formation of H_2O_2 by ORR process due to the presence of appropriate number of protons in the electrolyte, which demonstrates better performance in cleavage of the ether bonds than the superoxide radicals.

ACKNOWLEDGEMENTS
This project was supported by Beijing Natural Science Foundation (No.2182046).

References

1. R. Rinaldi, R. Jastrzebski, M.T. Clough, J. Ralph, M. Kennema, P.C. Bruijnincx, B.M. Weckhuysen, *Angew. Chem., Int. Ed.*, 55 (2016) 8164.
2. Strassberger Z, Tanase S, Rothenberg G, *RSC Adv.*, 4 (2014) 25310.
3. Galkin M V, Samec J S, *ChemSusChem*, 9 (2016) 1544.
4. S. Gillet, M. Aguedo, L. Petitjean, A.R.C. Morais, A.M.D. Lopes, R.M. Lukasik, P.T. Anastas, *Green Chem.,* 19 (2017) 4200.
5. Chatel G, Rogers R D, *ACS Sustainable Chem. Eng.*, 2 (2016) 322.
6. J.Y. Kim, J. Park, U.J. Kim, J.W. Choi, *Energy Fuels*, 29 (2015) 5154.
7. H. Wang, H. Wang, E. Kuhn, M.P. Tucker, B. Yang, *ChemSusChem*, 11 (2018) 285.
8. J. Wang, W. Li, H. Wang, Q. Ma, S. Li, H.M. Chang, H. Jameel, *Bioresour. Technol.*, 243 (2017) 100.
9. Y. Huang, L. Li, A. Zheng, Z. Zhao, H. Li, *Energy Fuels*, 31 (2017) 12263.
10. M. Zhang, F.L.P. Resende, A. Moutsoglou, *Fuel*, 116 (2014) 358.
11. M.M. Jensen, D.T. Djajadi, C. Torri, H.B. Rasmussen, R.B. Madsen, *ACS Sustainable Chem. Eng.*, 6 (2018) 5940.
12. Z. Yuan, S. Cheng, M. Leitch, *Bioresour. Technol.*, 101(2010)9308.
13. S. Dabral, J.G. Hernandez, P.C.J. Kamer, C. Bolm, *ChemSusChem*, 10 (2017) 2707.
14. R. Ma, M. Guo, X. Zhang, *Catal. Today*, 302 (2018) 50.
15. Z. Fang, M.S. Meier, *Org. Biomol. Chem.*, 16 (2018) 2330.
16. D. Shao, J. Liang, X. Cui, H. Xu, W. Yan, *Chem. Eng. J.*, 244 (2014) 288.
17. Y.S. Wang, F. Yang, Z.H. Liu, L. Yuan, G. Li, *Catal. Commun.*, 67 (2015) 49.
18. X. Hao, Y. Quansheng, S. Dan, Y. Honghui, L. Jidong, F. Jiangtao, Y. Wei, *J. Hazard. Mater.,* 286 (2015) 509.
19. D. Di Marino, V. Aniko, A. Stocco, S. Kriescher, M. Wessling, *Green Chem.*, 19 (2017) 4778.
20. P. Cai, H. Fan, S. Cao, J. Qi, S. Zhang, G. Li, *Electrochim. Acta,* 264 (2018) 128.
21. S. Stiefel, J. Lölsberg, L. Kipshagen, R. Möller-Gulland, M. Wessling, *Electrochem. Commun.,* 61 (2015) 49.
22. R. Tolba, M. Tian, J. Wen, Z.H. Jiang, A. Chen, *J. Electroanal. Chem.*, 649 (2010) 9.
23. K. Pan, M. Tian, Z. H. Jiang, B. Kjartanson, A. Chen, *Electrochim. Acta,* 60 (2012) 147.
24. D. Shao, J.D. Liang, X.M. Cui, H. Xu, W. Yan, *Chem. Eng. J.*, 244 (2014) 288.
25. E. Reichert, R. Wintringer, D.A. Volmer, R. Hempelmann, *Phys. Chem. Chem. Phys.*, 14 (2012) 5214.
26. O. Movil-Cabrera, A. Rodriguez-Silva, C. Arroyo-Torres, J.A. Staser, *Biomass Bioenergy*, 88 (2016) 89.

27. Moodley B, Mulholland D A, Brookes H C, *Water S A,* 31 (2011) 569.
28. L. Wang, Y.M. Chen, S.Y. Liu, H.M. Jiang, L.N. Wang, Y.Z. Sun, P.Y. Wan, *RSC Adv.*, 7 (2017) 51419.
29. H.B. Zhu, Y.M. Chen, T. F. Qin, L. Wang, Y. Tang, Y.Z. Sun, and P. Y. Wan, *RSC Adv.*, 4 (2014) 6232.
30. H.B. Zhu, L. Wang, Y.M. Chen, G.Y. Li, H. Li, Y. Tang, and P. Y. Wan, *RSC Adv.*, 4 (2014) 29917.
31. C. Pozo-Gonzalo, A.A.J. Torriero, M. Forsyth, D.R. MacFarlane, P.C. Howlett, *J. Phys. Chem. Lett.*, 4 (2013) 1834.
32. B. Martiz, R. Keyrouz, S. Gmouh, M. Vaultier, V. Jouikov, *Chem. Commun.,* 6 (2004) 674.
33. M. Hayyan, M.A. Hashim, I.M. AlNashef, *Ionics*, 21 (2015) 719.
34. J. Gebicki, A. Kloskowski, W. Chrzanowski, *Electrochim. Acta,* 56 (2011) 9910.
35. J. Lee, D.S. Silvester, *Analyst*, 141 (2016) 3705.
36. L. Wang, S.Y. Liu, H.M. Jiang, Y.Y. Chen, L.N. Wang, G.Y. Duan, Y.Z. Sun, Y.M. Chen, P.Y. Wan , *J. Electrochem. Soc.,* 165 (2018) H705.
37. X.Z. Yuan, V. Alzate, Z. Xie, D.G. Ivey, E. Dy, W. Qu, *J. Electrochem. Soc.*, 161 (2014) A458.
38. E.E. Switzer, R. Zeller, Q. Chen, K. Sieradzki, D.A. Buttry, C. Friesen, *J. Phys. Chem. C*, 117 (2013) 8683.
39. D. Zhang, T. Okajima, F. Matsumoto, T. Ohsaka, *J. Electrochem. Soc.*, 151 (2004) D31.
40. T.K.F. Dier, D. Rauber, D. Durneata, R. Hempelmann, D.A. Volmer, *Sci. Rep.*, 7 (2017) 5041.
41. A. Brandt-Talbot, F.J.V. Gschwend, P.S. Fennell, T.M. Lammens, B. Tan, J. Weale, J.P. Hallett, *Green Chem.*, 19 (2017) 3078.
42. G.A. Snook, A.S. Best, A.G. Pandolfo, A.F. Hollenkamp, *Electrochem. Commun.*, 8 (2006) 1405.
43. A. Khan, X. Lu, L. Aldous, C. Zhao, *J. Phys. Chem. C*, 117 (2013) 18334.
44. Z. Wu, M. Li, J. Howe, H. M. Meyer, S. H. Overbury, *Langmuir*, 26 (2010) 16595.